OPTICAL PROCESSES IN SINGLE-WALLED CARBON NANOTUBES THREADED BY A MAGNETIC FLUX

J. KONO,[1,†] S. ZARIC,[1] J. SHAVER,[1] X. WEI,[2] S. A. CROOKER,[3]
O. PORTUGALL,[4] G. L. J. A. RIKKEN,[4] R. H. HAUGE,[5] and R. E. SMALLEY[5]

[1]*Department of Electrical and Computer Engineering, Rice University, Houston, Texas 77005, U.S.A.* [†]*E-mail: kono@rice.edu*
[2]*National High Magnetic Field Laboratory, Florida State University, Tallahassee, Florida 32310, U.S.A.*
[3]*National High Magnetic Field Laboratory, Los Alamos National Laboratory, Los Alamos, New Mexico 87545, U.S.A.*
[4]*Laboratoire National des Champs Magnétiques Pulsés, 31432 Toulouse Cedex 04, France*
[5]*Department of Chemistry, Rice University, Houston, Texas 77005, U.S.A.*

Single-walled carbon nanotubes threaded by a magnetic flux ϕ are predicted to posses novel magnetic and optical properties, critically depending on the value of ϕ/ϕ_0 where ϕ_0 is the magnetic flux quantum. This is a consequence of the Aharonov-Bohm phase $2\pi\phi/\phi_0$ influencing the boundary conditions on the Bloch wavefunctions. Here we report results of a series of magneto-optical studies of micelle-suspended single-walled carbon nanotubes in aqueous solutions in high magnetic fields. Their exotic magnetic properties manifest themselves in near-infrared magneto-absorption and magneto-photoluminescence spectra, including static and dynamic magnetic linear dichroism, splittings of exciton peaks, and field-induced band gap shrinkage. We show that these observations are quantitatively consistent with existing theories based on the Aharonov-Bohm effect.

Keywords: carbon nanotubes; Aharonov-Bohm effect; magnetic flux quantum.

1. Introduction

The states of Bloch electrons are affected by a magnetic field in a non-trivial manner when the magnetic length is comparable to, or smaller than, the lattice constant. In such high fields, their energy spectra exhibit intriguing fine structures as a function of the number of magnetic flux quanta ($\phi_0 = e/h$) per unit cell.[1] In a single-walled carbon nanotube (SWNT), a similar, but much simpler, phenomenon is expected to occur when a magnetic field is applied parallel to the tube axis.[2] Namely, the band gap of a SWNT is predicted to oscillate between zero and a finite value as a function of magnetic flux ϕ with period ϕ_0; i.e., a SWNT can be either a metal or an insulator, depending on ϕ/ϕ_0. This exotic behavior is a direct consequence of the Aharonov-Bohm (AB) phase influencing the circumferential boundary condition on the Bloch wavefunction.

Here we present results of our recent magneto-optical experiments on carbon nanotubes in high DC and pulsed magnetic fields,[3,4,5] which provide the first experimental evidence for the influence of the Aharonov-Bohm phase on the electronic states of SWNTs. Due to the small diameters (∼1 nm) and the relatively large room temperature linewidth of SWNTs (∼20 meV) used in these experiments, a very high magnetic field is required to make the predicted phenomena clearly visible.

Through near-infrared absorption and photoluminescence (PL) spectroscopies in DC magnetic fields up to 45 T,[3] we observed field-induced optical anisotropy (i.e., linear dichroism) as well as peak shifts and splittings. The amounts of shifts and splittings depend on the value of ϕ/ϕ_0 and are quantitatively consistent with existing theories. In particular, our data clearly demon-

strated that the band gap of semiconducting SWNTs with 1 nm diameter monotonically shrinks with magnetic field with a rate ∼1 meV / T. In addition, through detailed analysis of the magnetic field-dependence of the shifts and splittings, we determined the magnetic susceptibility anisotropy of semiconducting nanotubes.[4]

Furthermore, using pulsed magnetic fields up to 75 T,[5] we made a clear observation of absorption peak splittings, which show that the degeneracy between the K and K' points in graphene k-space can be lifted by the breakdown of the time-reversal symmetry caused by the application of a magnetic field. Finally, we present time dependent magneto-optical transmission measurements in pulsed fields up to 54 T. Polarized optical transmission in the Voigt geometry reveals time dependent optical anisotropy, indicating that the nanotubes can dynamically align in response to the millisecond time-scale pulsed fields. Unlike the previous studies with DC fields, however, the transmission dynamics show a time lag with respect to the field pulse, suggesting that nanotube alignment/de-alignment is hysteretic. These results imply that while magnetic fields can be used for manipulating nanotubes, it is necessary to take into account nanotube inertia as well as environmental properties in correctly understanding and predicting the magneto-alignment dynamics.

2. Theory

2.1. *The Aharanov-Bohm effect on nanotube band structure*

In the presence of a magnetic field B, the *generalized* periodic boundary condition in the circumferential direction is given by

$$\psi(\vec{r}+\vec{C_h}) = \psi(\vec{r})\exp(2\pi i\varphi), \qquad (1)$$

where $\varphi \equiv \phi/\phi_0$ and $\vec{C_h} = (n,m)$ is the chiral vector. On the other hand, because of the existence of the periodic potential along the circumference, the Bloch condition has to be satisfied, i.e.,

$$\psi(\vec{r}+\vec{C_h}) = \psi(\vec{r})\exp(i\vec{k}\cdot\vec{C_h}), \qquad (2)$$

where $\vec{k}$ is the Bloch vector. In order for Eqs. (1) and (2) to be simultaneously satisfied, $\vec{k}$ along the circumference has to be quantized as $\vec{k}\cdot\vec{C_h} = m+\varphi$, where m is an integer. Thus, allowed $\vec{k}$ states continuously and periodically change with the Aharonov-Bohm phase $2\pi\varphi$.

Using $\mathbf{k}\cdot\mathbf{p}$ theory, Ajiki and Ando solved an effective-mass equation near the K point to find[2]: $E_{\pm,n}(k) = \pm\gamma\sqrt{\kappa(n,\phi)^2+k^2}$, where $\gamma \approx 0.646$ eV·nm, $\kappa(n,\phi) = (2\pi/L)\,(n-\nu/3-\phi/\phi_0)$, $L = |\vec{C_h}|$, $n = 0,\pm1,...$ (subband index), and + (−) corresponds to the conduction (valence) band. Thus, the band gap is

$$E_g = 2\gamma|\kappa(0)| = \frac{4\pi\gamma}{L}\left|\frac{\phi}{\phi_0}-\frac{\nu}{3}\right|. \qquad (3)$$

At zero field ($\phi = 0$), E_g is zero for metallic ($\nu = 0$) nanotubes while $E_g = 4\pi\gamma/3L$ for type-I ($\nu = 1$) and type-II ($\nu = -1$) semiconducting nanotubes. These simple rules break down at finite magnetic fields ($\phi \neq 0$), and E_g exhibits oscillations with period ϕ_0, i.e., the magnetic flux quantum. Furthermore, since a magnetic field breaks the time-reversal symmetry, the degeneracy between the K and K' points is lifted. Specifically, for a type-I semiconducting nanotube, the lowest transition (E_{11}) splits into

$$E_g = \frac{4\pi\gamma}{3L}\left(1\pm\frac{3\phi}{\phi_0}\right). \qquad (4)$$

The magnitude of splitting is given by

$$\Delta_{AB} = 8\pi\gamma\phi/L\phi_0 = 2\gamma LB/\phi_0 \equiv vB \qquad (5)$$

Similar splitting is expected for higher subband transitions as well.[6,7,8,9,10] As a numerical example, let us consider a (10,3) tube, for which $\nu = 1$, $L = 2.936$ nm, and $E_g(\phi = 0) = 4\pi\gamma/3L = 0.922$ eV. Equation (5) then predicts a splitting of $\Delta_{AB} \approx 41$ meV at 45 T.

2.2. *Magnetic alignment*

Carbon nanotubes have anisotropic magnetic properties.[11] An interesting consequence of this is magnetic alignment. In fact, it is important to understand the angular distribution of nanotubes in the solution at each magnetic field value in order to extract the true AB splitting values from data.

While the splitting rate v [Eq. (5)] is defined for a nanotube parallel to the applied field, experimentally we observe an apparent splitting rate of an ensemble of nanotubes with an angular distribution characterized by the probability of finding a nanotube in an angular range relative to the B direction. At 0 T, the nanotubes are randomized in solution. In a magnetic field, the nanotubes align due to their magnetic anisotropy. The angular probability distribution is given (in spherical coordinates) by:

$$P_u(\theta)d\theta = \frac{\exp(-u^2\sin^2\theta)\sin\theta d\theta}{\int_0^{\pi/2}\exp(-u^2\sin^2\theta)\sin\theta d\theta} \quad (6)$$

where

$$u \equiv \sqrt{\frac{B^2N(\chi_\parallel - \chi_\perp)}{k_BT}}\ , \quad (7)$$

where $\chi_\perp$ and $\chi_\parallel$ are the diamagnetic susceptibilities per mole of carbon atoms in a nanotube along its two principal axes, and θ is defined as the angle between the nanotube long axis and the magnetic field.

Using Eq. (6), one can calculate the expectation value of any physical quantity that depends on the angle θ. One useful quantity is the so-called nematic order parameter,[12,13,14] defined as

$$S = (3\left\langle\cos^2\theta\right\rangle - 1)/2\ . \quad (8)$$

This parameter is 0 when the nanotubes are completely randomly oriented and 1 when all the nanotubes in the solution are pointing in the magnetic field direction. Figure 1 shows S calculated for DC fields. If a DC 100 T magnet existed, it would be ideal for aligning our small diameter SWNTs.

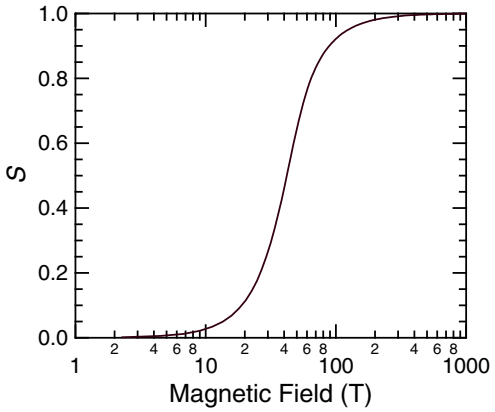

Fig. 1. Calculated steady state nematic order parameter, S. The magnetic susceptibility anisotropy[4] (1.4×10^{-5} emu/mol), average length (300 nm), diameter (1 nm), and temperature (300 K) were used in calculation.

3. Experimental

The samples studied in the present work were aqueous suspensions of individualized HiPco nanotubes produced at Rice. The samples were prepared by high sheer mixing of nanotubes in a 1 wt. % solution of surfactant (sodium dodecyl sulfate, sodium benzosulfonic acid, or sodium cholate) in D_2O, sonication, and centrifugation. The resulting supernatant was enriched in individualized SWNTs surrounded by surfactant micelles.[15] The nanotubes are thus unbundled and prevented from interacting with each other, which leads to chirality-dependent peaks in absorption and PL.[15,16]

We used a variety of high-field magnets for performing magneto-optical experiments. For DC field experiments a 10 T superconducting magnet (at Rice), a 33 T water-cooled magnet, and the 45 T hybrid magnet [both in Tallahassee, Florida] were used. Pulsed field experiments were conducted using capacitor bank driven magnets of 67 T (in Los Alamos, New Mexico), 54 T, and the 75 T ARMS magnet[17] (in Toulouse, France).

Samples were mounted on a specially designed stick with integrated optic fibers, lenses, mirrors, and polarizers. The nan-

otube solution was contained in a quartz cell with an effective optical length of 0.5 cm for absorption (0.1 cm for PL). Absorption spectra were normalized to a 1 wt. % surfactant in D_2O solution.

We used a Si charge coupled device (in the visible) and an InGaAs array detector (in the near-infrared). A quartz-tungsten-halogen lamp was used for the absorption measurements, and a Ti:Sapphire laser was used in the PL measurements. Experiments in pulsed fields were recorded with an exposure plus readout time of ∼1.5 ms, this resulted in spectra taken in ∼.5 T increments.

We utilized Voigt geometry with two different polarizations (P) for these experiments, $B \parallel P$ and $B \perp P$. Due to the samples being in aqueous suspensions, all measurements were done at room temperature.

4. Results

Absorption spectra in the near-infrared range are shown in Fig. 2 at various DC fields up to 45 T. The peaks in the specra correspond to the lowest-energy transitions (E_{11}) in semiconducting nanotubes with different chiralities. As the field increases, the $B \parallel P$ ($B \perp P$) absorption increases (decreases) as a result of magnetic alignment; note that the E_{11} transitions are allowed only for the light polarized parallel to the tube axis. At 45 T, while the $B \perp P$ absorption (sensitive to the nanotubes lying more perpendicular to the B) shows only peak broadening, the $B \parallel P$ absorption (sensitive to the nanotubes lying more parallel to B) shows more pronounced spectral changes. This can be successfully explained using our model (see the dotted lines, explained later) that takes into account magnetic alignment and AB splitting. However, clear absorption peak splittings cannot be seen even at 45 T.

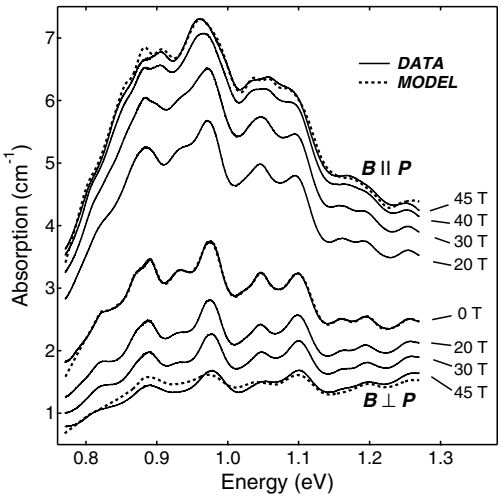

Fig. 2. Magnetic field induced anisotropy. Room temperature absorption of the SWNT sample was measured in Voigt geometry for two polarizations of the probe light: $B \parallel P$ ($B \perp P$). Dashed lines represent results of our model based on AB effect and the magnetic alignment. No intentional offset.

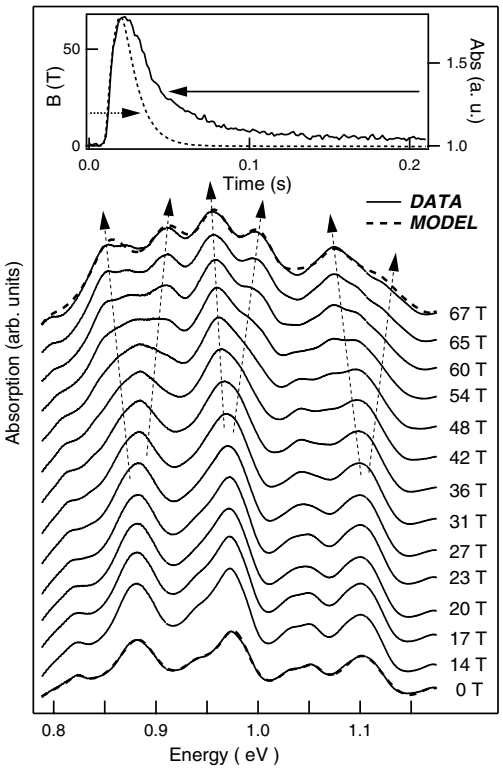

Fig. 3. Absorption spectra at various magnetic fields taken in the Voigt geometry with light polarization parallel to the field. The traces are offset for clarity. The inset shows relative change in absorption at 2.3 eV during a 67 T shot.

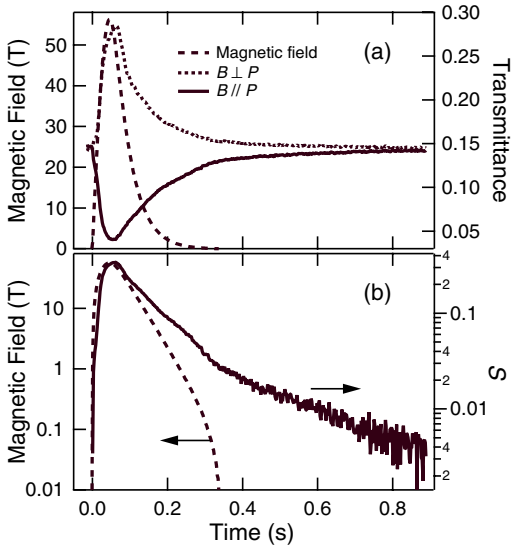

Fig. 4. Dynamic alignment. Transmission anisotropy in the second subband during a 54 T shot (a). S, calculated from anisotropy, plotted on a semilog scale shows characteristic relaxation time for nanotubes in solution.

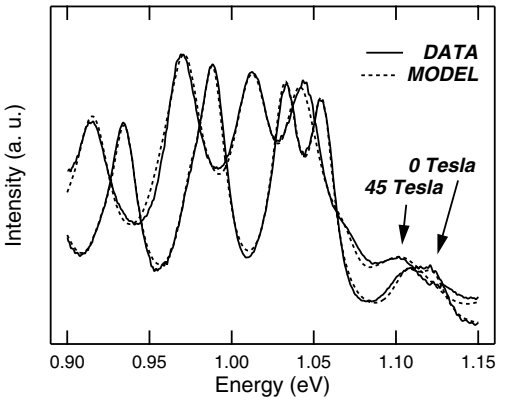

Fig. 5. PL spectra at 0 T and 45 T showing magnetic-field-induced band-gap shrinkage due to the Aharonov-Bohm effect. The data was taking with 790 nm excitation, and different peaks correspond to different chirality nanotubes.

The use of pulsed magnets allowed us to access higher fields. Figure 3 shows $B \parallel P$ absorption spectra taken during a 67 T magnetic pulse. At fields above 54 T, clear absorption peak splittings are observed. In addition, time-dependent polarized transmission allows for the observation of nanotube solution dynamics. Figure 4 shows a decrease (increase) in transmission for $B \parallel P$ ($B \perp P$) as field is applied. As the field increases the nanotubes begin to align reaching a maximum order parameter of $\sim$0.35 at 54 T. The 45 T DC case reaches a maximum order parameter of $\sim$0.5, indicating that the tubes do not completely align on fractional second time scales. This is due to many factors, including nanotube inertia (dependant on length and diameter) and environment (depending on solution viscosity and proximity of other nanotubes).

Figure 5 shows PL spectra at 0 T and 45 T. A 790 nm beam selectively excited four chiralities in the sample. This selectivity allows us to see much clearer spectral changes in PL data compared to absorption data. Namely, all peaks shift to lower energies as B is increased. The dotted lines are simulations based on our model taking into account the AB effect and magnetic alignment and explain the observations very well.

5. Discussion

In a magnetic field parallel to a nanotube axis, absorption and PL peaks are predicted to split by an amount proportional to the applied field [see Eq. (5)]. The absorption peaks are predicted to split into two equal height peaks with the separation proportional to B. PL peaks will split with the same splitting rate, but with the relative size of the two peaks determined by the Boltzmann factor.

The 0 T PL spectrum was fit using Lorentzian peaks that correspond to the chiralities present in the sample. The 45 T PL spectrum was then simulated by varying two parameters for each Lorentzian, u and v. The first parameter, u, describes the angular distribution of the nanotubes at a given B field [see Eq. (7)]. The second, v, is the rate of peak splitting with the field applied parallel to the nanotube [see Eq. (5)]. For any given θ this rate was multiplied by $\cos\theta$ to

account only for the flux component threading the nanotube. The different intensities of the split PL peaks were taken into account through a Boltzmann factor (with temperature $T = 300$ K). The best 45 T fit is shown as dotted lines in Fig. 5. The average splitting rate obtained in this way is $v = 0.9$ meV/T.

We use $a_{\parallel}^{(n,m)}(\hbar\omega, B)$ and $a_{\perp}^{(n,m)}(\hbar\omega, B)$ to denote the intrinsic absorption spectra (in $\mathrm{cm}^{-1}\mathrm{mole}^{-1}$) for (n, m) nanotubes in parallel magnetic field B when the light is polarized parallel and perpendicular to the long axis of the nanotube, respectively (where $\hbar\omega$ is the photon energy). Theoretically, $a_{\perp}^{(n,m)}(\hbar\omega, B)$ is predicted to be zero for E_{11} and E_{22} transitions due to the depolarization effect,[18] but we retain this quantity in the following formal derivation for the sake of completeness.

The intrinsic absorption spectra defined above are not directly obtainable from experiments due to the angular distribution of nanotubes. For example, the *measured* $B \parallel P$ absorption for (n, m) tubes is an average over the angular distribution of nanotubes given by

$$\bar{a}_{\parallel}^{(n,m)}(\hbar\omega, B) = \left\langle a_{\parallel}^{(n,m)} r^2 + a_{\perp}^{(n,m)}(p^2 + q^2) \right\rangle \cdot N^{(n,m)} \quad (9)$$

where $a_{\parallel}^{(n,m)}$ and $a_{\parallel}^{(n,m)}$ in the brackets are functions of $\hbar\omega$ and $B\cos\theta$, p, q (r) are the directional cosines between the polarization direction and the short (long) principal axes of the nanotube, and $N^{(n,m)}$ is the number of moles of (n, m) nanotubes. Similarly,

$$\bar{a}_{\perp}^{(n,m)}(\hbar\omega, B) = \left\langle \frac{1}{2} a_{\parallel}^{(n,m)} \sin^2\theta + a_{\perp}^{(n,m)}(1 - \sin^2\theta) \right\rangle \times N^{(n,m)} \quad (10)$$

We used Eqs. (9) and (10) (with $a_{\perp}^{(n,m)} = 0$) to simulate our absorption data. At 0 T, Eq. (9) becomes:

$$\bar{a}_{\parallel}^{(n,m)}(\hbar\omega, 0T) = a_{\parallel}^{(n,m)}(\hbar\omega, 0T)\langle\cos^2\theta\rangle = \frac{1}{3} a_{\parallel}^{(n,m)}(\hbar\omega, 0T) \cdot N^{(n,m)}, \quad (11)$$

which relates $a_{\parallel}^{(n,m)}(\hbar\omega, B\cos\theta) \cdot N^{(n,m)}$ at 0 T with the measured 0 T absorption. The 67 T absorption can then be simulated using Eq. (9) by fitting parameters $u^{(n,m)}$ and $v^{(n,m)}$ as in the PL simulations.

When fitting the 0 T absorption data, several closely spaced (n, m) peaks might be fitted as a wider absorption peak. Nevertheless, this simulation yields data that agrees well with the measured data [see Fig. (3)] and yielded (n, m)-averaged $u = 1.9$ and $v = 0.7$ meV/T. The same model was then applied to the 45 T data [see Fig. (2)]. This treatment again yielded an average splitting rate of 0.7 meV/T. Furthermore, keeping the same fitting parameters, the $B \perp P$ data was successfully reproduced at 45 T (see Fig. 2).

The inset in Fig. 3, as well as the data in Fig. 4(a), shows that the absorption change does not exactly follow the applied pulse, i.e., there is a lag between the peak field and peak alignment. Thus, while the pulsed field data in Fig. 3 are explained well using the angular distribution given by Eq. 6, u is no longer given by Eq. 7, but is now a mere parameter. Finally, in Fig. 4(b), magnetic field and nematic order parameter are plotted on a semilog scale. It can be seen that the residual alignment persists even after the field goes to zero. This shows that nanotube inertial effects and solution viscosity must be accounted for when measuring nanotube alignment dynamics.

6. Conclusions and Future work

We have observed the modification of states of Bloch electrons by an Aharonov-Bohm phase in SWNTs by magneto-optical spectroscopy. We also investigated both DC and dynamic magnetic alignment of SWNT so-

lutions. There are still many questions that need to be explored such as solution dynamics, temperature, other geometries and polarizations, and higher field dependences.

When analyzing dynamic alignment data by plotting on a semilog scale it becomes apparent that this is a form of pump-probe spectroscopy. The short field pulse prepares the nanotubes in an aligned state (magnetic pump), while the transmission probes the relaxation dynamics (optical probe). This data can be analyzed to enlighten the inertial and environmental effects on the thermal motion of the nanotubes in solution. Analysis of data on samples with different lengths and bundling states is underway.

We are also expanding this work with destructuve pulsed magnets up to 150 T in Los Alamos and up to 300 T at Humboldt University in Berlin. We have already completed single wavelength solution dynamics work in Berlin,[19] and magneto-absorption measurements are currently in progress. Aligned nanotube gel films, fabricated by several-groups, are ideal for ultrahigh field and low temperature magneto-optics studies. Film samples can be aligned, cooled, are solid, and are very thin. These characteristics bypass alignment convolution, temperature restrictions, allow for easy handling and smaller, simpler sample holders.

Acknowledgements

This work was supported in part by the Robert A. Welch Foundation (through Grant No. C-1509) and the National Science Foundation (through Grant Nos. DMR-0134058, DMR-0325474, and INT-0437342). A portion of this work was performed at the National High Magnetic Field Laboratory, which is supported by NSF Cooperative Agreement No. DMR-0084173 and by the State of Florida. We thank V. I. Klimov for the use of his InGaAs detector for measurements in Los Alamos. We also thank G. N. Ostojic, V. C. Moore, and M. Furis for technical assistance.

References

1. D. R. Hofstadter, Phys. Rev. B **14**, 2239 (1976).
2. H. Ajiki and T. Ando, J. Phys. Soc. Jpn. **62**, 1255 (1993).
3. S. Zaric, G. N. Ostojic, J. Kono, J. Shaver, V. C. Moore, M. S. Strano, R. H. Hauge, R. E. Smalley, and X. Wei, Science **304**, 1129 (2004).
4. S. Zaric, G. N. Ostojic, J. Kono, J. Shaver, V. C. Moore, R. H. Hauge, R. E. Smalley, and X. Wei, Nano Lett. **4**, 2219 (2004).
5. S. Zaric, G. N. Ostojic, J. Shaver, J. Kono, O. Portugall, P. H. Frings, G. L. J. A. Rikken, M. Furis, S. A. Crooker, X. Wei, V. C. Moore, R. H. Hauge, and R. E. Smalley, Phys. Rev. Lett., to appear (cond-mat/0509429).
6. T. Ando, Semicond. Sci. Technol. **15**, R13 (2000).
7. T. Ando, J. Phys. Soc. Jpn. **73**, 3351 (2004).
8. T. Ando, J. Phys. Soc. Jpn. **74**, 777 (2005).
9. S. Roche, G. Dresselhaus, M. S. Dresselhaus, and R. Saito, Phys. Rev. B **62**, 16092 (2000).
10. F. L. Shyu, C. P. Chang, R. B. Chen, C. W. Chiu, and M. F. Lin, Phys. Rev. B **67**, 045405 (2003).
11. J. Kono and S. Roche, "Magnetic Properties," in *Carbon Nanotubes: Properties and Applications*, ed. M. J. O'Connell (CRC Press, Boca Raton, 2006, to be published).
12. M. Fujiwara, N. Fukui, and Y. Tanimoto, J. Phys. Chem. B **103**, 2627 (1999).
13. M. F. Islam, D. E. Milkie, C. L. Kane, A. G. Yodh, and J. M. Kikkawa, Phys. Rev. Lett. **93**, 037404 (2004).
14. Y. Murakami, E. Einarsson, T. Edamura, and S. Maruyama, Phys. Rev. Lett. **94**, 087402 (2005).
15. M. J. O'Connell, S. M. Bachilo, C. B. Huffman, V. C. Moore, M. S. Strano, E. H. Haroz, K. L. Rialon, P. J. Boul, W. H. Noon, C. Kittrell, J. Ma, R. H. Hauge, R. B. Weisman, and R. E. Smalley, Science **297**, 593 (2002).
16. S. M. Bachilo, M. S. Strano, C. Kittrell, R. H. Hauge, R. E. Smalley, and R. B. Weisman, Science **298**, 2361 (2002).
17. H. Jones, P. H. Frings, M. von Ortenberg,

A. Lagutin, L. V. Bockstal, O. Portugall, and F. Herlach, Physica B **346-347**, 553 (2004).
18. H. Ajiki and T. Ando, Physica B **201**, 349 (1994).
19. J. Shaver, J. Kono, S. Hansel, A. Kirste, M. von Ortenberg, C. H. Mielke, O. Portugall, R. H. Hauge, and R. E. Smalley, in: *Narrow Gap Semiconductors 2005, Proceedings of the Twelfth International Conference on Narrow Gap Semiconductors*, eds. J. Kono and J. Léotin (Institute of Physics, Bristol, 2005, to be published).